

A QUASI-ANALYTICAL MODEL FOR REMOTE FIELD EDDY CURRENT INSPECTION

A. Musolino*, R. Rizzo, and E. Tripodi

Department of Energy and System Engineering, Largo L. Lazzarino, Pisa 56123, Italy

Abstract—The Remote Field Eddy Current (RFEC) method is widely used to inspect both ferrous and nonferrous metal tubes when internal access is the only possible way of inspection. An axisymmetric quasi-analytical model is presented in this paper in order to simulate the behavior of a RFEC system during its operation. The proposed model, based on the application of the Fourier Transform in space, is able to take into account the finite length of the excitation coil, fed by an AC current, and the relative movement between the RFEC system and the wall tube. Numerical simulations based on integral formulations and experimental measurements were used to validate the proposed quasi-analytical model.

1. INTRODUCTION

Non Destructive Testing (NDT) is a continuously growing subject. Today available NDT technologies exploit several physical principles: ultrasound [1], eddy current [2], thermal analysis [3] etc. The Remote Field Eddy Current (RFEC) technique is widely used since it is able to detect both internal and external defects in pipes, with low frequency excitation, when internal access is the only possible method of inspection. The excitation and the detection coils are placed inside the tube at a distance of two or three tube diameter from each other (Remote-Field Zone). The field produced by the excitation coil traverses the tube wall twice before it reaches the detection coil. In order to allow this process, the penetration depth related to the frequency of the current on the excitation coil must be of the same order as the tube wall thickness. The adopted frequency usually ranges

Received 11 September 2012, Accepted 24 October 2012, Scheduled 25 October 2012

* Corresponding author: Antonino Musolino (musolino@dsea.unipi.it).

from a few Hz to a few hundreds of Hz. It is then possible to extract information about wall thickness, presence of defects and metal loss due to corrosion [4–9].

The analysis and design of RFEC systems are usually carried out by using numerical tools. Although they are able to produce accurate results, numerical models often require long computations. In particular, in the optimization process, when a great number of evaluations of the objective function is required, the use of numerical tools may result in unviable times. The availability of analytical or quasi-analytical models, as the one proposed in this paper, reduces the computation time and provides a useful tool for the validation of numerical methods. Obtaining a full analytical model is prevented in the present case by the necessity of performing a numerical inverse Fourier transform. As far as the numerical tools, let us observe that the distance between the excitation coil and the remote field detection coil makes the use of Finite Elements Method (FEM) difficult due to the need to mesh the external tube region and extend it to “infinity” [9–16]. Furthermore, the relative speed between the coils and the tube is not easy to manage by FEM due to the presence of sliding meshes and as a consequence this method may result in long computation time.

Alternative approaches, mostly based on integral formulations [17–24], have a number of characteristics that make them well suited for the analysis of these geometries. In particular, integral formulations require the discretization of the active regions only and the problem of coupling meshes with different speed is absent. The Method of Moments (MoM) is one of the most used integral formulation. The numerical results reported in this paper have been obtained by a MoM approach where the governing equations are reformulated in terms of an equivalent network. Such an approach allows the use of robust and efficient algorithms for the sensitivity analysis with respect to the design parameters of the device. This greatly helps in the development of the system [25, 26] especially when optimization by gradient based methods is adopted.

In this paper, we use a quasi-analytical method to model the electromagnetic phenomena that occur in RFEC operation involving axisymmetric defects. By using the Fourier Transform, the solution of the governing equations in terms of the magnetic vector potential can be expressed by means of Bessel functions. After a numerical inverse Fourier transform the distribution of the magnetic flux density and of the current density distributions in the regions of interest is obtained. The model also takes into account the presence of uniform, symmetrical defects by considering an auxiliary problem and applying the superposition procedure.

2. MODELING THE RFEC TECHNIQUE

An RFEC system, shown schematically in Figure 1(a), is composed of an excitation coil and a detection coil, both inside the tube and at a distance of about two or three tube diameters far away each other [4–6]. The excitation coil is energized with low frequency AC.

Two distinct coupling paths exist between the excitation and the detection coils. The direct path, inside the tube, is rapidly attenuated by the circumferential eddy currents induced in the tubes wall. It can be assimilated to an evanescent mode in waveguides. If the detection coil is far enough from the excitation coil the coupling through the direct path is negligible and the detected signal is due to an indirect coupling path. Near the excitation coil the field diffuses radially outward through the wall; it is attenuated and its phase is shifted. Once outside this energy is guided axially along the outer wall with reduced attenuation. In the remote field zone (2–3 tube diameters), the field outside the tube is greater than the field inside, that is almost entirely due to the field diffusing back (inside the tube) from the outside. If we consider that the indirect path is characterized by a double through-wall transit, we can easily recognize how anomalies anywhere in the indirect path cause changes in the magnitude and phase of the detected signal. This qualitative picture of the RFEC effect can be formalized as in [27], where the mutual impedance of two coils, both inside a conductive tube is examined in details. By using the Fourier transform this impedance can be decomposed into two kind of terms: some representing the waveguide modes (associated with the poles of the Fourier transform of the impedance) and others representing the outgoing flux density (associated with the branch point singularities of the Fourier transform). In the remote field zone the terms that dominate the mutual impedance expression are the second ones.

2.1. The Superposition Procedure

In order to find an analytical expression of the electromagnetic field distributions in the described RFEC system, a procedure based on the superposition of different solutions was developed.

Let us consider Figure 1 which shows an example of the geometry and excitation encountered in the RFEC technique applications. The regular domain Ω is the cylindrical tube, while Γ represents the defect. We assume that both Ω and Γ have cylindrical symmetry. For the considered configuration, we suppose that two analytical solutions referred to the same regular domain Ω exist. The first is the solution of problem a) (Figure 1(b)) expressing the fields and

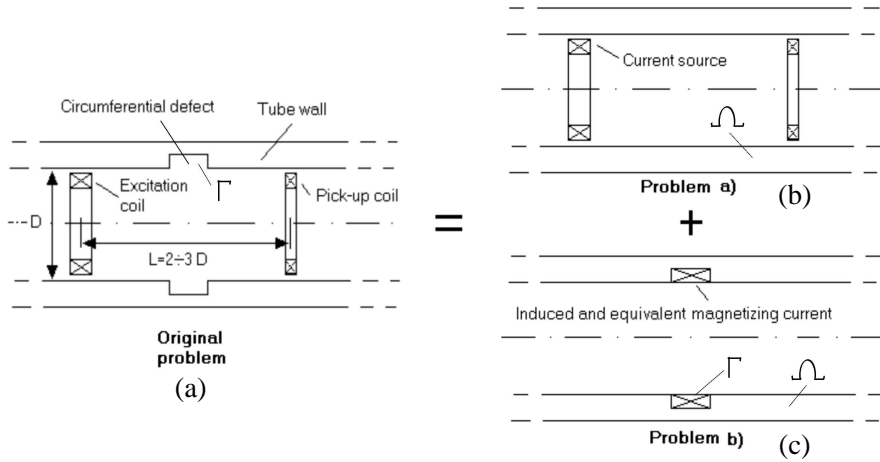


Figure 1. Schematic representation of an RFEC system and problem decomposition.

currents everywhere as a function of the sinusoidal current source in the moving coil. Problem b) (Figure 1(c)) is an auxiliary problem obtained by setting the current source to zero and considering as excitation terms the induced and the magnetization currents (with the opposite sign) obtained from the solution of problem a) in the subregion Γ (the defect).

The auxiliary problem is solved in the original regular domain Ω , i.e., the tube without the defect. The superposition of the two solutions of problems a) and b), while forcing the resulting currents in the subregion Γ to zero, provides the solution of the problem in the original domain.

In case of presence of multiple defects, an auxiliary problem is defined for each defect (considering it as the only one), and the superposition procedure is applied by summing the solution related to the no-defect geometry with the solutions of the auxiliary problems.

2.2. The Quasi-analytical Model

Figure 2 reports a schematic radial representation of the RFEC system, used for the deduction of the quasi-analytical model [28–31].

Problem a): in order to solve this problem, we can substitute the excitation coil with an equivalent current sheet properly positioned and characterized by the same amperturns.

After introducing the vector potential \bar{A} with the Coulomb gauge

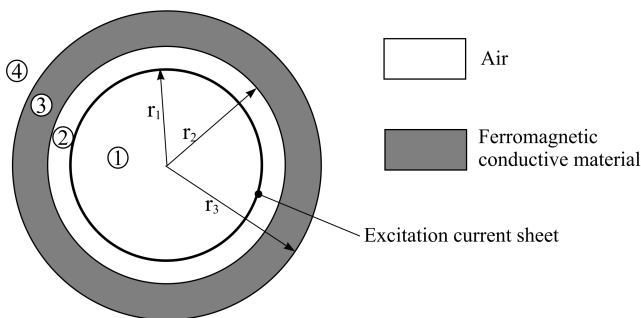


Figure 2. Schematic radial representation of the RFEC system.

$\nabla \cdot \bar{A}$ in the Maxwell equations, the field equation of an isotropic medium moving with velocity v is the following:

$$\nabla^2 \bar{A} = \mu\sigma \left(\frac{\partial}{\partial t} \bar{A} - v \times (\nabla \times \bar{A}) \right) \quad (1)$$

where μ and σ respectively indicate the permeability and conductivity of the medium. The current density \bar{J}_1 (in A/m²) of the excitation current sheet can be written as:

$$\bar{J}_1(r, \varphi, z, t) = J_1 \sin(\omega t) [u(z - v_z t) - u((z + \Delta z) - v_z t)] \delta(r - r_1) \cdot \bar{a}_\varphi \quad (2)$$

where \bar{a}_φ indicates the azimuth direction. $u(z)$ is the unit step function, $\delta(r - r_1)$ the Dirac function located at the middle point of the radial dimension of the excitation coil, Δz the axial dimension of the excitation coil, t the time, and v_z the velocity of the test tool. Furthermore, ω represents the angular frequency of the excitation current, and J_1 (in A/m) is the amplitude of equivalent current sheet obtained as total current in the excitation coil divided by its axial dimension Δz .

In the present problem, the vector potential has only azimuth components in cylindrical coordinates and is a function of r , z and t : $\bar{A} = A_\varphi(r, z, t) \cdot \bar{a}_\varphi$.

By substituting in (1), after some manipulations we obtain:

$$\frac{\partial^2 A_\varphi}{\partial r^2} + \frac{1}{r} \frac{\partial A_\varphi}{\partial r} + \frac{\partial^2 A_\varphi}{\partial z^2} - \frac{A_\varphi}{r^2} = \mu\sigma \left(\frac{\partial A_\varphi}{\partial t} + v_z \frac{\partial A_\varphi}{\partial z} \right) \quad (3)$$

Under sinusoidal steady state condition, the vector potential is expressed as: $A_\varphi(r, z, t) = A_\varphi(r, z) \cdot e^{j\omega t}$, where $j = \sqrt{-1}$. By substituting in (3) we obtain:

$$\frac{\partial^2 A_\varphi}{\partial r^2} + \frac{1}{r} \frac{\partial A_\varphi}{\partial r} + \frac{\partial^2 A_\varphi}{\partial z^2} - \frac{A_\varphi}{r^2} = \mu\sigma \left(j\omega A_\varphi + v_z \frac{\partial A_\varphi}{\partial z} \right) \quad (4)$$

Let the Fourier transform of $A_\varphi(r, z)$ with respect to z be denoted by $\tilde{A}_\varphi(r, \zeta)$:

$$A_\varphi(r, z) = \frac{1}{2\pi} \int_{-\infty}^{+\infty} \tilde{A}_\varphi(r, \zeta) e^{j\zeta z} d\zeta \quad (5)$$

By substituting (5) in (4), and introducing the subscript i to indicate the regions in which (4) is written (see Figure 2), we obtain:

$$\frac{\partial^2 \tilde{A}_{i,\varphi}}{\partial r^2} + \frac{1}{r} \frac{\partial \tilde{A}_{i,\varphi}}{\partial r} - \left(\zeta^2 + \frac{1}{r^2} \right) \tilde{A}_{i,\varphi} = j\mu\sigma(\omega + \zeta v_z) \tilde{A}_{i,\varphi} \quad (6)$$

Equation (6) can be written in the general form:

$$\frac{\partial^2 \tilde{A}_{i,\varphi}}{\partial r^2} + \frac{1}{r} \frac{\partial \tilde{A}_{i,\varphi}}{\partial r} - \left(h_i^2 + \frac{1}{r^2} \right) \tilde{A}_{i,\varphi} = 0 \quad (7)$$

where: $h_i^2 = \zeta^2$ for $i = 1, 2, 4$, and $h_i^2 = \zeta^2 + j\mu\sigma(\omega + \zeta v_z) = j\alpha^2$ for $i = 3$.

The solutions of Equation (7) are expressed in terms of modified Bessel functions of the first and second kind:

$$\tilde{A}_{i,\varphi} = c_i I_1(\zeta r) + c'_i K_1(\zeta r); \quad \text{for } i \neq 3 \quad (8)$$

$$\tilde{A}_{3,\varphi} = c_3 I_1(\sqrt{j}\alpha r) + c'_3 K_1(\sqrt{j}\alpha r); \quad \text{for } i = 3 \quad (9)$$

The determination of the unknown coefficients in the previous relations is performed by imposing the normal conditions and the boundary conditions on the interfaces 1-2, 2-3, and 3-4 (Figure 2). The normal component \tilde{B}_\perp of the magnetic flux density \tilde{B} must be continuous across the interfaces 1-2, 2-3 and 3-4; the tangential component \tilde{H}_\parallel of the magnetic field \tilde{H} must be continuous across the interfaces 2-3, and 3-4. Because of the presence of the excitation current sheet, \tilde{H}_\parallel is discontinuous across the interface 1-2. Due to the axialsymmetry of the problem, the normal component is the radial one, and the tangential component is the axial one.

$$\begin{aligned} \tilde{B}_{\perp i}(r_i) &= \tilde{B}_{\perp i+1}(r_i); \quad \text{for } i = 1, 2, 3; \\ \tilde{H}_{\parallel i}(r_i) &= \tilde{H}_{\parallel i+1}(r_i); \quad \text{for } i = 2, 3; \\ \tilde{H}_{\parallel i}(r_1) &= \tilde{H}_{\parallel i+1}(r_1) + \tilde{J}(r_1); \quad \text{for } i = 1; \end{aligned} \quad (10)$$

where $\tilde{J}_1(\zeta) = j \frac{\tilde{J}_1}{\zeta} (j e^{j\zeta \Delta z} - 1)$ is the Fourier transform of the excitation current.

In order to obtain the integration coefficients c_i and c'_i , the fields \tilde{B} and \tilde{H} are expressed in terms of the Fourier transformed vector potential \tilde{A} .

Due to the asymptotic behavior of the modified Bessel function we have: $c'_1 = c_4 = 0$. The other coefficients are obtained by solving a set of six linear algebraic equations obtained by (10). The following expressions can be written:

$$c_i = \tilde{J}_1(\zeta) \frac{N_i(\zeta)}{D_i(\zeta)}; \quad c'_i = \tilde{J}_1(\zeta) \frac{N'_i(\zeta)}{D'_i(\zeta)}; \quad (11)$$

where $N_i(\zeta)$, $D_i(\zeta)$, $N'_i(\zeta)$ and $D'_i(\zeta)$ are involved expressions containing Bessel functions. They can be obtained by using a symbolic solver for the linear system (10).

Finally, a numerical Fourier inverse transform allows the vector potential to be obtained as well as all the other electromagnetic quantities in the whole space.

Problem b): once the magnetic vector potential and the magnetic flux density are known everywhere in the configuration without the defect, the induced currents ($\bar{J}_i(r, z) = -j\sigma(\omega - \beta_n v_z)\bar{A}$) and equivalent magnetizing currents ($\bar{J}_m(r, z)$, as defined below) may be found in the region occupied by the defect. Problem b) is set up by placing these currents in the region occupied by the defect. If the defect has small axial and radial dimensions, a uniform value for the induced currents in this region can be assumed; otherwise, if the defect is not small enough, a piecewise-constant function for the source of the auxiliary problem can be considered and the solution can be found by summing the contributions of these constant terms.

As well known, the magnetizing equivalent currents are composed by two terms: the volume and the surface current densities.

The first one is evaluated by taking the curl of the magnetizing vector \bar{M} found through the following equations:

$$\bar{M} = \frac{\mu_r - 1}{\mu_0 \mu_r} \bar{B}; \quad \bar{J}_{vol,m} = \bar{\nabla} \times \bar{M}; \quad (12)$$

where μ_r is the material relative magnetic permeability, and the subscript *vol* refers to the “volume” equivalent magnetizing currents.

Since the $\bar{J}_{vol,m}$ is homogeneous with \bar{J}_i and both are defined in the same region, they can be superimposed. In the hypothesis of small defect we consider a uniform current density distribution $\bar{J}_{vol}(r_0, z_0)$ at the domain center (r_0, z_0) as shown in Figure 3(a). This current is obtained as $\bar{J}_{vol}(r_0, z_0) = -\bar{J}_{vol,m}(r_0, z_0) - \bar{J}_i(r_0, z_0)$.

As the final step of the procedure, the surface equivalent magnetization currents ($\bar{J}_{surf,m}$) need to be taken into account due to the magnetization discontinuity on the defect boundary. These currents are obtained as:

$$\bar{J}_{surf,m} = \bar{M} \times \bar{a}_n; \quad (13)$$

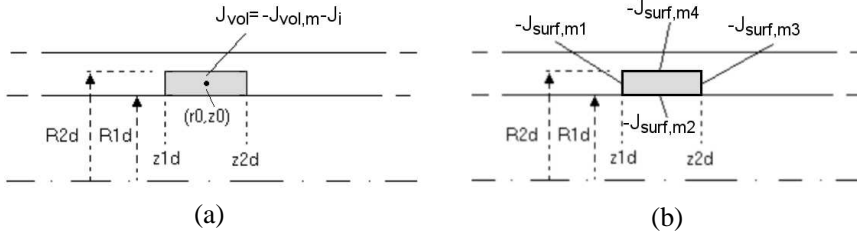


Figure 3. Equivalent magnetization currents: (a) volume and (b) surface.

where \bar{a}_n is a unit vector pointing out of the closed surface representing the boundary of the defect region Γ .

Under the assumption of cylindrical symmetry, the surface magnetization currents have azimuth components only.

As shown in Figure 3(b), we assume a constant surface current for small defects. By applying the same method adopted for the other current terms, we find the last term of solution b).

3. RESULTS

The described model was applied to a ferromagnetic tube having an internal diameter of 60 mm, a wall thickness of 7 mm, a relative permeability of 190 and a conductivity of 10.5×10^6 S/m. The analysis of the problem was performed by simulating a circumferential defect of 5 mm in axial dimension and 2 mm in radial dimension on both the inner and outer walls of the pipe. Calculations were made for an excitation coil of about 2000 AmperTurns (#18 AWG – $\phi \simeq 1$ mm) at a frequency of 20 Hz and moving at a speed $v_z = 2$ m/s. The results obtained by the quasi-analytical procedure described above were compared with those obtained from the integral formulation and with measured data. A research computer code, developed at the Department of Energy and System Engineering, University of Pisa, Italy, has been used to simulate the behavior of the proposed configuration. The code is based on an integral 3-D formulation that reduces the field analysis to an equivalent network analysis. The active regions only (conductors and magnetic materials, if present) are discretized by using elementary volumes, and an equivalent network is built. The currents in the branches of the network are mapped into the currents flowing in the elementary volumes. This allows a straightforward analysis of massive 3-D devices coupled with lumped circuits. The details of the general formulation are reported in [32–35].

Figure 4(a) refers to the case of an internal defect and reports the values of the current distribution along the axial direction of the pipe at 1 mm inside the inner wall of the pipe.

Figure 4(b) refers to the case of an internal defect and shows the profile of the axial component of magnetic flux density B just inside the tube, as a function of the distance from the excitation coil, normalized with respect to the internal diameter ID. The agreement between the values obtained from the proposed method and from

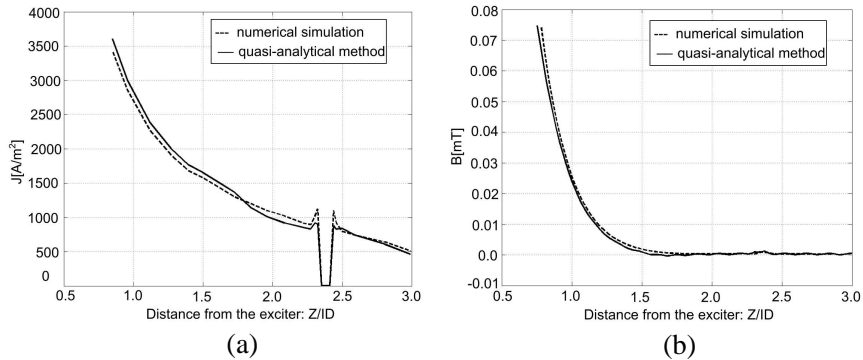


Figure 4. Computed results for an internal defect as a function of distance from the excitation coil, inside the pipe at 1 mm from the inner surface. (a) Induced current density distribution. (b) Axial component of the magnetic flux density distribution.

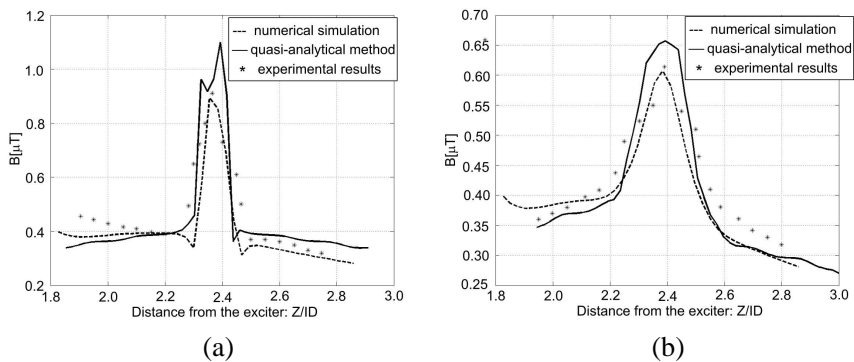


Figure 5. Comparison of numerical and experimental results for the axial component of B around defects positioned at about $Z/ID = 2.3$. (a) Inner defect. (b) Outer Defect.

integral formulation is highly satisfactory.

Figures 5(a) and 5(b) refer to the case of an inner and outer defect, respectively, and both show an enlarged portion of the profile of the axial component of flux density at a distance of about $2.3 \cdot ID$ from the excitation coil. Figure 5(a) is obtained from Figure 4(b) as they refer to the same configuration.

In both Figures 5(a) and 5(b), the axial component profiles of B obtained from the quasi-analytical model are compared with those obtained from the numerical model and with experimental data taken on a pipe sample with an artificial defect. The differences between simulated results are within 10% and both are in good agreement with the measured data.

4. CONCLUSIONS

A quasi-analytical model for Remote Field Eddy Current inspection in linear materials has been described. The simulations carried out showed that the model is able to analyze a class of RFEC problems involving axisymmetric defects, allowing the determination of all the electromagnetic quantities. The results obtained by the proposed quasi-analytical method were compared with those obtained by a numerical formulation and with experimental data taken on a pipe sample. The comparison was highly satisfactory and revealed that the described model represents a useful tool in the Non Destructive Testing context and it can be advantageously used in the validation of numerical codes.

REFERENCES

1. Musolino, A., M. Raugi, M. Tucci, and F. Turcu, "Time, wavelet and Hilbert-Huang domain analysis of signals from ultrasonic based equipment for the non destructive evaluation of concrete and brick masonry walls," *International Conference on Computational Science and Its Applications 2008*, Vol. 1, 566–581, Perugia, Jun. 30–Jul. 3, 2008.
2. Mahmoudi, M. and S. Y. Tan, "Depth detection of conducting marine mines via eddy-current and current-channeling response," *Progress In Electromagnetics Research*, Vol. 90, 287–307, 2009.
3. Subbarao, G. V. and R. Mulaveesala, "Quadratic frequency modulated thermal wave imaging for non-destructive testing," *Progress In Electromagnetics Research M*, Vol. 26, 11–22, 2012.

4. Schmidt, T. R., "The remote field eddy current inspection technique," *Materials Evaluation*, Vol. 42, 225–230, 1984.
5. Atherton, D. L., "Remote field eddy current inspection," *IEEE Trans. Magn.*, Vol. 31, No. 6, 4142–4147, Nov. 1995.
6. Kobayashi, N., S. Ueno, S. Nagai, M. Ochiai, and N. Jimbo, "Remote field eddy current testing for steam generator inspection of fast reactor," *Nuclear Engineering and Design*, Vol. 241, No. 12, 4643–4648, Dec. 2011.
7. Rebican, M., Z. Chen, N. Yusa, K. Miya, T. Uchimoto, and T. Takagi, "Investigation of numerical precision of 3-D RFECT signal simulations," *IEEE Trans. Magn.*, Vol. 41, No. 5, 1968–1971, May 2005.
8. Duchesne, S., N. Bouzida, and J. P. Villeneuve, "Performance estimation of a remote field eddy current method for the inspection of water distribution pipes," *J. Water Resour. Plann. Manage.*, Vol. 137, No. 6, 521–530, 2011.
9. Thirunavukkarasu, S., B. P. C. Rao, T. Jayakumar, and B. Raj, "Techniques for processing remote field eddy current signals from bend regions of steam generator tubes of prototype fast breeder reactor," *Annals of Nuclear Energy*, Vol. 38, No. 4, 817–824, Apr. 2011.
10. Atherton, D. L., W. Czura, and D. A. Lowther, "Open-boundary finite element calculations for remote field eddy current systems," *IEEE Trans. Magn.*, Vol. 26, No. 5, 2863–2865, Sep. 1990.
11. Wang, H., Q. Luo, X. Wang, G. Tian, L. Xing, P. Wang, and Y. Li, "Simulation and experimental study of remote field eddy current testing on flat conductive plate," *Int. J. Appl. Electromagn. Mech.*, Vol. 33, No. 3, 1261–1266, 2010.
12. Di Puccio, F., A. Musolino, R. Rizzo, and E. Tripodi, "A self-controlled maglev system," *Progress In Electromagnetics Research M*, Vol. 26, 187–203, 2012.
13. Thirunavukkarasu, S., B. P. C. Rao, S. Mahadevan, T. Jayakumar, B. Raj, Z. Zeng, L. Udpa, and S. S. Udpa, "Finite element modeling for detection of localized defects using remote field eddy current technique," *Journal of Research in Non destructive Evaluation*, Vol. 20, No. 3, 145–258, 2009.
14. EFFE v2.00, *User Manual*, Bathwick Electrical Design Ltd., UK, Sep. 2009.
15. Rizzo, R., N. Sgambelluri, E. P. Scilingo, M. Raugi, and A. Bicchi, "Electromagnetic modeling and design of haptic interface prototypes based on magnetorheological fluids," *IEEE*

- Trans. Magn.*, Vol. 43, No. 9, 3586–3598, Sep. 2007.
16. Bicchi, A., M. Raugi, R. Rizzo, and N. Sgambelluri, “Analysis and design of an electromagnetic system for the characterization of magneto-rheological fluids for haptic interfaces,” *IEEE Trans. Magn.*, Vol. 41, No. 5, 1876–1879, May 2005.
 17. Musolino, A. and R. Rizzo, “Numerical analysis of brush commutation in helical coil electromagnetic launchers,” *IET Science, Measurement and Technology*, Vol. 5, No. 4, 147–154, Jul. 2011.
 18. Musolino, A. and R. Rizzo, “Numerical modeling of helical launchers,” *IEEE Trans. on Plasma Sci.*, Vol. 39, No. 3, 935–940, Mar. 2011.
 19. Di Puccio, F., R. Bassani, E. Ciulli, A. Musolino, and R. Rizzo, “Permanent magnet bearings: Analysis of plane and axisymmetric V-shaped element design,” *Progress In Electromagnetics Research M*, Vol. 26, 205–223, 2012.
 20. Barmada, S., A. Musolino, M. Raugi, and R. Rizzo, “Force and torque evaluation in hybrid FEM-MOM formulations,” *IEEE Trans. Magn.*, Vol. 37, No. 5, 3108–3111, Sep. 2001.
 21. Musolino, A., R. Rizzo, E. Tripodi, and M. Toni, “Modeling of electromechanical devices by GPU-accelerated integral formulation,” *Int. J. Numer. Model.*, 1–21, Wiley Online Library, wileyonlinelibrary.com, DOI:10.1002/jnm.1860, 2012.
 22. Musolino, A., R. Rizzo, E. Tripodi, and M. Toni, “Acceleration of electromagnetic launchers modeling by using graphic processing unit,” *IEEE 16th EML Symposium Conference Proceedings*, Vol. 1, 1–6, Beijing, May 15–19, 2012.
 23. Barmada, S., A. Musolino, M. Raugi, and R. Rizzo, “Numerical simulation of a complete generator-rail launch system,” *IEEE Trans. Magn.*, Vol. 41, No. 1, 369–374, 2005.
 24. Barmada, S., A. Musolino, M. Raugi, and R. Rizzo, “Analysis of the performance of a combined coil-rail launcher,” *IEEE Trans. Magn.*, Vol. 39, No. 1, 103–107, 2003.
 25. Barmada, S., A. Musolino, M. Raugi, R. Rizzo, and M. Tucci, “A wavelet based method for the analysis of impulsive noise due to switch commutations in power line communication (PLC) systems,” *IEEE Trans. Smart Grid*, Vol. 2, No. 1, 80–89, Mar. 2011.
 26. Barmada, S., A. Musolino, R. Rizzo, and M. Tucci, “Multi-resolution based sensitivity analysis of complex non-linear circuits,” *IET Circuits, Devices and Systems*, Vol. 6, No. 3, 176–

- 186, 2012.
27. Haugland, M., "Fundamental analysis of the remote-field eddy current effect," *IEEE Trans. Magn.*, Vol. 32, No. 4, 3195–3211, 1996.
 28. Musolino, A., R. Rizzo, and E. Tripodi, "Analysis and design criteria of a tubular linear induction motor for a possible use in the electro-magnetic aircraft launch system," *IEEE 16th EML Symposium Conference Proceedings*, Vol. 1, 1–6, Beijing, May 15–19, 2012.
 29. Musolino, A., R. Rizzo, and E. Tripodi, "Tubular linear induction machine as a fast actuator: Analysis and design criteria," *Progress In Electromagnetics Research*, Vol. 132, 603–619, 2012.
 30. Mukerji, S. K., D. S. Srivastava, Y. P. Singh, and D. V. Avasthi, "Eddy current phenomena in laminated structures due to travelling electromagnetic fields," *Progress In Electromagnetics Research M*, Vol. 18, 159–169, 2011.
 31. Musolino, A., R. Rizzo, and E. Tripodi, "Analytical model of a travelling wave multipole field electromagnetic launcher," *IEEE 16th EML Symposium Conference Proceedings*, Vol. 1, 1–6, Beijing, May 15–19, 2012.
 32. Barmada, S., A. Musolino, R. Rizzo, and A. Tellini, "Field analysis in axisymmetric actuators," *IEEE Trans. Magn.*, Vol. 36, No. 4, 1906–1909, 2000.
 33. Musolino, A., "Finite-element method/method of moments formulation for the analysis of current distribution in rail launchers," *IEEE Trans. Magn.*, Vol. 41, No. 1, 387–392, 2005.
 34. Musolino, A., M. Raugi, and B. Tellini, "3-D field analysis in tubular induction launchers with armature transverse motion," *IEEE Trans. Magn.*, Vol. 35, No. 1, 154–159, 1999.
 35. Barmada, S., A. Musolino, M. Raugi, and R. Rizzo, "Analysis of the performance of a multi-stage pulsed linear induction launcher," *IEEE Trans. Magn.*, Vol. 37, No. 1, 111–115, Jan. 2001.